Quantification of laser local hyperthermia induced by gold plasmonic nanoparticles

Alexander N. Yakunin
Yuri A. Avetisyan
Valery V. Tuchin

Quantification of laser local hyperthermia induced by gold plasmonic nanoparticles

Alexander N. Yakunin,[a,b,][*] Yuri A. Avetisyan,[a,b] and Valery V. Tuchin[a,b]
[a]Russian Academy of Sciences, Institute of Precise Mechanics and Control, 24 Rabochaya Street, Saratov 410028, Russia
[b]N.G. Chernyshevsky Saratov State University, 83 Astrakhanskaya Street, Saratov 410012, Russia

Abstract. This paper discusses one of the key problems of laser-induced tissue/cell hyperthermia mediated by gold nanoparticles, namely, quantifying and precise prediction of the light exposure to provide a controllable local heating impact on living organisms. The distributions of such parameters as an efficiency factor of absorption, differential and integral absorbing power of a nanoparticle, temperature increment, and Arrhenius damage integral were used to quantify nanoparticle effectiveness in the two-dimensional coordinate space "laser wavelength $(\lambda) \times$ radius of gold nanoparticles (R)." It was found that the fulfillment of required spatial and temporal characteristics of temperature fields in the vicinity of nanoparticle determines the optimal λ and R. As a result, the area in the space $(\lambda \times R)$ with a minimal criticality to alterations of the local hyperthermia may be significantly displaced from the position of the plasmonic resonance. The aspects of generalization of the proposed methodology for the analysis of local hyperthermia using nanoparticles of different shapes (nanoshells, nanorods, nanostars) and short pulse laser radiation are discussed. © 2015 Society of Photo-Optical Instrumentation Engineers (SPIE) [DOI: 10.1117/1.JBO.20.5.051030]

1 Introduction

The development of novel laser-based therapeutic technologies using nanoparticles,[1–3] such as local hyperthermia, including treatment of cancer tumors,[1,3–8] targeted drug delivery,[1,2,9] and cell optoporation,[10–13] requires quantification of CW or pulsed laser irradiation and local thermal effects in tissues and cells doped by the nanoparticles. The creation of a quantitative system of objective justification and prognosis of photothermal effects induced by CW or short pulse lasers is of great importance.[1–14] In recent years, the effectiveness of nanoparticle permeability into cells[13,15,16] and distribution of the electromagnetic field near the nanoparticles depending on their form has been intensively studied.[3,17,18] There are also available various optical imaging modalities, such as spatially resolved reflectance measurements, optical coherence tomography, and IR radiometry, which are capable to monitor nanoparticle distributions in tissues and tissue overheating in average.[3,5–8,19–21]

For many applications related to cell optoporation and cancer cell killing, a localized overheating of biological medium around particle surface and its kinetics should be quantified. In particular, the improvement of the spatial resolution in determining of local thermal effects induced by laser radiation of individual nanoparticles was studied.[22] A significant shift in plasmon resonance frequency caused by changes of the shape, size, or configuration of closely spaced nanoparticles was found by the authors of Ref. 22. These changes caused by melting or defragmentation of nanoparticles when irradiated by a laser pulse of high intensity need to be controlled. Measurement of the resonance absorption shift allows one to increase resolution of the nonlinear photothermal microscopy

from 50–100 to 10–20 nm.[23] Nanoparticle clustering and nonlinear processes at irradiation by laser pulses increase sharpness of photothermal and photoacoustic spectral resonances.[24] In this paper, the existence of the initial peak of the photothermal signal associated with the rapid nanoparticle heating was found in a picosecond range, the subsequent cooling has duration of nano- and microseconds, and the increase of laser intensity led to nonlinear processes caused by the formation of nanobubbles around the superheated nanoparticles. The method of selective thermomechanical destruction of cancer cells induced by nanobubbles created at laser irradiation at the wavelength of maximal absorption of plasmonic nanoparticles was recently patented.[25]

The DNA catenane systems (interlocked DNA rings) as molecular DNA machines for the programmed, reversible, and switchable arrangement of different-sized gold nanoparticles (GNPs) were recently introduced.[26] The GNP structures revealing unique emerging switchable spectroscopic features, such as plasmonic coupling or surface-enhanced fluorescence, were demonstrated.

The efficiency of light-to-thermal energy conversion of gold and some other metallic nanoparticles under optical irradiation was described in Refs. 27 and 28. It was found that maximal nanoparticle temperature can be achieved for a nanoparticle in which absorption efficiency factor is smaller than its maximal value.

This brief review shows that for different applications of plasmonic nanoparticles, a precise quantification of laser heating of the nanoparticle and surrounding medium is important and not yet totally understood. For some prospective applications, low/moderate laser intensities with prolonged exposures

*Address all correspondence to: Alexander N. Yakunin, E-mail: anyakunin@mail.ru

can be effective, because it may induce various local biological effects, such as cell apoptosis or cell membrane enhanced permeability, without harmful impact on surrounding cells and tissue structures free from nanoparticles. Therefore, in this paper, we present the analytical approach combined with Arrhenius damage (impact) integral to quantify precisely hyperthermia and biological impact in the conditions, when the exposure time is tens to hundreds of seconds, and the generated heat affects an area of tens to hundreds of nanometers in the vicinity of the nanoparticle.

2 Description of the Model

We consider a GNP of a spherical shape with radius R in a tissue or cell structure, which is presented as an aquatic environment. This approach is widely used at modeling of thermal processes in biological tissues and cell structures (see, for example, Refs. 29–33 and the links in these articles). It is acquitted due to a slight difference of thermophysical properties of tissues and water.[19] For the simplicity, we have considered that optical and thermal properties of cell membrane and environment are similar. Using the spectral dependence of complex refractive index of gold[34] and real refractive index of water,[35] we have calculated initially the factors of efficiency of extinction Q_{ext}, scattering Q_{sca}, and absorption Q_{abs} of light by a particle, which are dimensionless quantities. Taking into account the size dependence of the dielectric function of the nanoparticles[36,37] in the framework of Mie theory (see, for example, Refs. 29 and 38) one obtains

$$Q_{abs} = Q_{ext} - Q_{sca}, \tag{1}$$

$$Q_{ext} = \frac{2}{x^2}\sum_{l=1}^{\infty}(2l+1)\mathrm{Re}(a_l + b_l), \tag{2}$$

$$Q_{sca} = \frac{2}{x^2}\sum_{l=1}^{\infty}(2l+1)(|a_l|^2 + |b_l|^2),$$

$$a_l = \frac{m\psi_l(y)\psi_l'(x) - \psi_l(x)\psi_l'(y)}{m\psi_l(y)\xi_l'(x) - \xi_l(x)\psi_l'(y)},$$

$$b_l = \frac{\psi_l(y)\psi_l'(x) - m\psi_l(x)\psi_l'(y)}{\psi_l(y)\xi_l'(x) - m\xi_l(x)\psi_l'(y)}. \tag{3}$$

Here, $x = 2\pi n(R/\lambda)$, $y = 2\pi N(R/\lambda)$, where n and N are refractive indices of the surrounding medium and the GNP, respectively, λ is the illuminating light wavelength in vacuum, $m = N/n$, ψ_l and ξ_l are the Riccati–Bessels functions, and the primes stand for derivatives.

The light energy absorbed by the nanoparticle per time unit has the dimension of power and is defined as

$$W_{abs} = Q_{abs}S_{\perp}I, \tag{4}$$

where $S_{\perp} = \pi R^2$ is the cross-sectional area of the nanoparticle of radius R, I is the light intensity. The volumetric density of this characteristic has the dimension of power per volume unit and is defined as

$$U_{abs} = \frac{W_{abs}}{V}, \tag{5}$$

where $V = (4/3)\pi R^3$ is the nanoparticle volume.

The steady-state bioheat equation, originated from the energy balance, describes the change in tissue temperature, $T(\mathbf{r})$, at point $\mathbf{r}$ in the tissue:[19,39,40]

$$\nabla[k_T \nabla T(\mathbf{r})] + S(\mathbf{r}) + \rho_b c_b q_b [T_a - T(\mathbf{r})] = 0, \tag{6}$$

where k_T is the local value of thermal conductivity inside the tissue (W/K); $S(\mathbf{r})$ is the heat source term (W/m^3) at point $\mathbf{r}$; ρ_b is the blood density (kg/m^3); c_b is the blood specific heat (J/kg K); q_b is the blood perfusion rate (1/s), defined as the volume of blood flowing through unit volume of tissue in one second; and T_a is the arterial blood temperature (K).

At neglecting of blood perfusion impact on the temperature distribution within the vicinity of the spherical GNP and assumption of spherical symmetry of the problem, Eq. (6) is transformed to

$$\frac{1}{r^2}\frac{\partial}{\partial r}\left[k_T r^2 \frac{\partial T(r)}{\partial r}\right] + S(r) = 0. \tag{7}$$

Here, $T(r)$ is the desired temperature at the distance r from the center of the nanoparticle, $k_T = k$ and $S(r) = U_{abs}$ inside GNP $(r \leq R)$, while $k_T = k_m$ and $S(r) = 0$ outside GNP $(r > R)$, k and k_m are the thermal conductivity of gold and water, respectively.

The solution of the heat conduction Eq. (7) must satisfy the continuity of temperature and normal component of heat flux at the boundaries of the contacting media (GNP—environment). The desired solution is

$$T(r) = T_0 + \begin{cases} \frac{U_{abs}R^2}{6k}\left[1 + 2\frac{k}{k_m} - \left(\frac{r}{R}\right)^2\right], & \text{for } r \leq R, \\ \frac{U_{abs}R^3}{3k_m}\frac{1}{r}, & \text{for } r \geq R. \end{cases} \tag{8}$$

Here, T_0 is the temperature of the environment far away from the GNP ($T_0 = 310$ K). In the particular case of $r = R$, we obtain from Eq. (8) the formula of Refs. 27 and 28 for temperature on the surface of GNP at "long pulse" regime. The part of Eq. (8) for $r > R$ describes the thermal diffusion in medium surrounding GNP.

We have to note that Eq. (8) is valid only for an infinite, spatially homogeneous medium surrounding a single nanoparticle. The heterogeneity of the medium (tissue boundaries, layered structure, complex cell structure, etc.) as well as the presence of nanoparticle clusters will lead to the nonapplicability of this equation. In this case, the calculation of the complex temperature fields can be done by using a numerical finite element method.[30–32] However, the main goal of this study is to analyze the local hyperthermia of the environment near the nanoparticles. Many of tissues and cells on the nanometer scale can be considered as homogeneous in absorption and index of refraction media in comparison with the strong optical inhomogeneity introduced by the nanoparticles. Absorption coefficient of gold is ~10^5 to 10^6 cm^{-1}, and relative index of refraction is ~0.15 to 1.28 in the visible/NIR wavelength range.[34] For soft tissues or cells, absorption coefficient is ~0.01 to 0.1 cm^{-1}, and relative index of refraction is ~1.05 to 1.10 for similar wavelength range.[19] Therefore, to account for actual tissue or cell structure environment, one will be able to correct only the amount of the bulk density of light energy within the region where the particle is located. For many tissues, strong light scattering provides the so-called diffusion regime[19] when any

nanoparticle, located deep in the tissue, will get even lighting from all sides. Another extreme case is transparent tissues, such as the cornea,[19] to which this approach can be applied directly. Relevant to the skin and many other turbid tissues, light scattering can be accounted for in the framework of the radiative transfer theory or Monte Carlo modeling.[19] By this, the light fluxes within the tissue will be connected with the incident light parameters at the entrance of a tissue slab, while maintaining the rest of the main stages of the present simulation the same.

3 Simulation Results and Discussion

3.1 Evaluation of GNP Heating Efficiency via Absorbed Power

As the initial evaluation criterion for GNP heating efficiency, the parameter Q_{abs} can be taken.[38] In the framework of the Mie theory, calculations over a wide range of wavelengths of the incident light λ from 320 to 1400 nm and nanoparticle radius R from 2 to 100 nm were performed. The results of calculations are shown in Fig. 1 in the form of topograms. This graphic representation allows one to understand specific features of interaction of the incident light with GNPs, which appear in the form of nanoparticle absorbed power and correspondingly in the local temperature increase around the particle.

The overall behavior of absorption efficiency Q_{abs} demonstrates the sensitivity to change both the light wavelength and the particle size [Fig. 1(a)]. This characteristic has a sharp maximum at the wavelength of 520 nm and nanoparticle radius of 38 to 40 nm. This is a result of existence of surface plasmon resonance (SPR) for GNPs induced by collective oscillatory motion of conduction electrons in the nanoparticle (see, for example, Refs. 2 and 38).

Parameters, Q_{abs}, Q_{sca}, and Q_{ext}, calculated for spherical GNPs at a few laser wavelengths can be found in literature.[29] The obtained dependences that account for the size effects are also in good agreement with the data on Q_{ext} presented in Ref. 2. The SPR phenomenon is one of the fundamental bases of laser-induced hyperthermia of tissues doped by nanoparticles.[1,2,5–7,18,25,27–33,41–45] Namely, SPR absorption of laser radiation caused by collective oscillations of electrons in the nanoparticle material, described by Eqs. (1)–(3), provides

a broad use of GNPs in different fields of biology and medicine.[1,2,5–7,10–18,21–33,41–45]

At the same time, we draw attention to the existence of a wide plateau around the exact resonance at its half-maximum. This plateau has a rather large area in coordinates λ–R: for wavelength range from less than 320 nm to 520 nm and for GNP radius from ∼40 nm to more than 100 nm. At the wavelengths above 720 nm in the entire NIR region and throughout the considered range of nanoparticle radius, 2 to 100 nm, the absorption efficiency Q_{abs} is of more than two orders of magnitude lower.

The distribution of volumetric density of heating power U_{abs} can be considered as an alternative criterion of nanoparticle heating efficiency. Figure 2 shows a plot for normalized (dimensionless) parameter U_{abs}/U_{abs0} in $\lambda \times R$-coordinates. The calculations were executed at $I = 100$ kW/cm² with $U_{abs0} = 1.0 \times 10^{17}$ W · m⁻³ as a scaling factor equal to the maximum of U_{abs} in the considered region of ($\lambda \times R$)-space. The behavior of U_{abs}/U_{abs0} maximal value takes the form of "ridge," stretched along R-axis.

The third criterion of the heating efficiency is the normalized integral thermal power of a single nanoparticle loading (dimensionless) W_{abs}/W_{abs0} (Fig. 3). Here, $W_{abs0} = 5.2 \times 10^{-5}$ W is a scaling factor equal to the maximum of W_{abs} in the ($\lambda \times R$)-space.

From the W_{abs}/W_{abs0}-topogram, it follows that this criterion gives a distinct advantage of large nanoparticles (to 100 nm) in a wide range of wavelengths less than 530 nm. In the region corresponding in Fig. 1 to the SPR (530 nm), now only poorly expressed signs of the local maximum, about three times lower than the global maximum, are seen. It becomes clear that the volume of nanoparticle is the predominant factor for heating efficiency, as SPR plays a leading role only for relatively small nanoparticles.

The further calculations of temperature increment will clarify the origin of the correlation of the considered criteria with the photothermal efficiency.

3.2 Evaluating the GNP Heating Efficiency by Induced Temperature Field

From the calculations of the temperature increment on the nanoparticle surface regarding T_0 (temperature of tissue far away from the GNP, for living body $T_0 = 310$ K), $\Delta T = T - T_0$
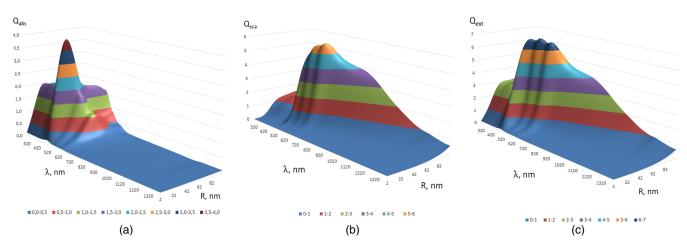

Fig. 1 Distribution of the efficiency of absorption Q_{abs} (a), scattering Q_{sca} (b), and extinction Q_{ext} (c) of the gold nanoparticle (GNP) versus wavelength λ and nanoparticle radius R.
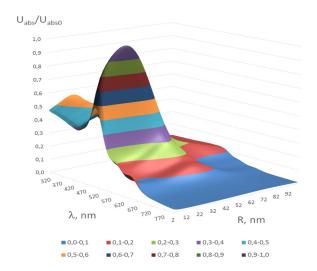
Fig. 2 Distribution of the normalized volumetric density of the heating power U_{abs}/U_{abs0} of the nanoparticle versus the light wavelength λ and the nanoparticle radius R.

given in Fig. 4, it follows that ΔT in two areas, where SPR exists and where large nanoparticles contributed are substantially equal. The likelihood that temperature generated by a large NP at a certain wavelength far from SPR may exceed temperature of a smaller NP with a strong SPR is also noted in Refs. 27 and 28. General view of topogram ΔT in Fig. 4 differs markedly from the topograms in Figs. 1–3. Evidently, the distribution Q_{abs} in Fig. 1(a) has a bimodal maximum also; however, character of the peaks differs greatly from that in Fig. 4, where the plateau transforms into an extended rather steep slope with a maximum at large R. The ratio of the two maxima in Fig. 4 is opposite to that in Fig. 1(a). The comparison of topograms is presented in Figs. 2 and 4, and Figs. 3 and 4 allow one to reveal similar differences in the form of maxima and at their altitudes. The observed conversion of topograms is determined by the obvious relationships:
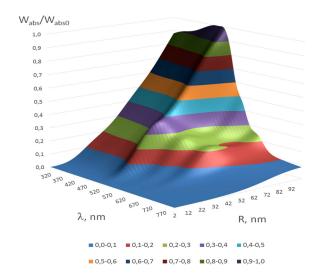

Fig. 3 Distribution of the normalized integral heating power of the nanoparticle W_{abs}/W_{abs0} versus the light wavelength λ and the nanoparticle radius R.
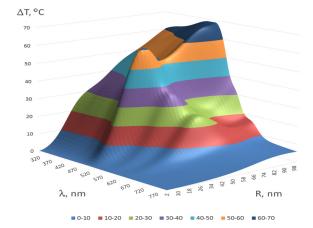

Fig. 4 Distribution of the temperature increment ΔT on the surface of the nanoparticle versus wavelength λ and nanoparticle radius R.

$$U_{abs} \sim Q_{abs}/R, \quad W_{abs} \sim Q_{abs} \cdot R^2,$$
$$\Delta T(r = R) \sim Q_{abs} \cdot R \sim W_{abs}/R. \tag{9}$$

Within the SPR region, the integrated power absorbed by a nanoparticle W_{abs} is about three times lower than the power absorbed by a big nanoparticle (see Fig. 3). However, ΔT is inversely proportional to R for a given W_{abs}. As a result, we get approximately an equivalent thermal effect (in terms of maximal temperature achievement) for these two practically important conditions (Fig. 4).

The temperature increment at a distance apart from nanoparticle surface in surrounding medium depends on nanoparticle size as well (Fig. 5). Near the surface of the nanoparticle within the distance, $\Delta r = 10$ nm plasmon-resonant nanoparticle provides ΔT about 10% less than a large one. As the distance from the nanoparticle increases, this difference also became bigger. At the distance $\Delta r = 100$ nm, ΔT is 40% and at $\Delta r = 1000$ nm—60% less. Therefore, plasmon-resonant nanoparticles are less effective in heating of the surrounding medium. In general, with increase of distance r, ΔT-distribution (see Fig. 5) becomes similar to distribution of the normalized integral heating power of a single nanoparticle W_{abs}/W_{abs0} in Fig. 3.

3.3 Evaluation of the Efficiency of GNPs by the Criterion of Arrhenius Damage Function

Thermal impact on tissues or cells is often used to provide therapeutic or biological effects, such as ablation of a tumor or coagulation a gastric ulcer, or cell laser optoporation and DNA transfection using lasers.[1,2,5–7,10–18,21–33,41–45] In all these and many other optothermal technologies, we are able to estimate the time-temperature exposure that will cause a particular thermal transition.[39,40,46] The variety of thermal transitions includes very slow low-temperature exposures, such as thermally triggered heat shock protein expression, to the fast high-temperature exposures required to coagulate collagen fibers.[46] Van der Waals, hydrogen, ionic, disulfide, and covalent molecular bonds may be broken during these thermal transitions. As it was shown in Ref. 46, the rate of such transitions is characterized by the number of bonds being cooperatively broken, and for the most irreversible thermal transitions, simultaneous breakage of many bonds is characteristic. Exposure time versus exposure temperature to achieve thermal damage for different types of
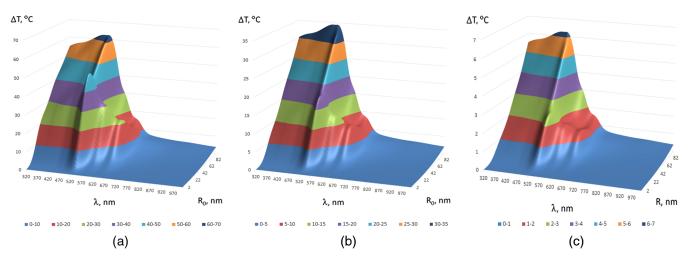
Fig. 5 Distribution of the temperature increment ΔT in the medium versus wavelength λ and nanoparticle radius R at a distance $\Delta r = 10$ nm (a); $\Delta r = 100$ nm (b); $\Delta r = 1000$ nm (c) from the particle surface.

transitions, such as induced heat shock protein expression, cell membrane damage, cell apoptosis, tissue necrosis, dermal shrinkage, collagen birefringence loss, collagen coagulation, etc., are in a wide range of time (from 10^{-8} to 10^5 s) and temperature (from 40°C to 140°C) exposures.[39,40,44,46]

If the concentration of GNPs is high and other nanoparticles are in the area of thermal impact of the nanoparticle under consideration, then the summation of thermal fields is necessary with the contribution of each of these GNPs. The area around the nanoparticle of radius r_a, within which impact is negligible, for example $\Delta T(r_a)/\Delta T(r_a = R) \leq 0.01$, can be introduced as "the zone of thermal impact of a nanoparticle." From Eq. (8), it follows that for GNP of $R = 2$ nm, $r_a = 0.2$ μm, and for GNP of $R = 100$ nm $r_a = 10$ μm, i.e., in the limits of a single cell or its organelles. For simplicity of consideration, but without loss of generality, we assume that in the zone of thermal impact of the nanoparticle, other nanoparticles are absent. This assumption in quite reasonable for many biomedical applications.[44]

The possibility of applying the stationary Eq. (8) to consider laser exposures τ of tens to hundreds seconds follows from numerical estimates of transient temperature field during heating of nanoparticle and its environment.[30–32] It was found that for a pulse duration $\tau_p \geq 100$ ns, temperature difference within the area of thermal impact of the GNP becomes stationary throughout the investigated range of particle size $R = 2 \div 100$ nm.

The irreversible thermal damage of a particular type is described by the Arrhenius rate process (Arrhenius function or integral) with the corresponding parameters[39,40,46]

$$\Omega(\mathbf{r}, \tau) = A \int_0^\tau \exp\left[-\frac{E_a}{\Re T(\mathbf{r}, t)}\right] dt, \qquad (10)$$

where A (s^{-1}) is the rate at which the native form molecule moves to a transition state atop an energy barrier of a particular chemical reaction, such as protein denaturation, $\exp\{E_a/[\Re T(\mathbf{r}, t)]\}$ is the dimensionless function characterizing the probability that the molecule will convert from the transition state to the denatured state, E_a (J/mol) is the activation energy, $\Re$ is the gas constant [8.314 J/(mol · K)], T is the temperature expressed in Kelvin (K) ($T = 273.15 + T$°C), $\mathbf{r}$ is the radius

vector of an arbitrary point in the space of interest, τ is the exposure time.

The dependence of the damage accumulation rate, defined as time derivative of the Arrhenius function $d\Omega/d\tau$, on temperature is shown in Fig. 6(a). For these calculations, parameters $A = 3.1 \cdot 10^{98}$ s^{-1} and $E_a = 6.3 \cdot 10^5$ J/mol that characteristic for pig skin damage were used.[40] The damage critical temperature T_{crit}, defined as temperature at $d\Omega/d\tau = 1$, is equal to 59.7°C.[40] The $d\Omega/d\tau$ function represents the rate of growth of tissue damage with temperature. The corresponding exposure time needed for 100%-damage of pig skin versus stationary temperature exposure is presented in Fig. 6(b). These data illustrate the criticality of thermal impact (threshold effect) relative to the temperature exposure.

As it was already pointed out, various photothermal processes can be described using Arrhenius function,[46] including the increased permeability of the cell membrane at its local thermal damage provided by hot metallic nanoparticles that are heated by laser irradiation.[10–13,31,33,47,48] The temperature exposure providing this damage is determined by the time exposure during which the irreversible phase transitions are distributed throughout the entire thickness of the cell membrane and some area along membrane around the nanoparticle connecting with the cell membrane. Therefore, it is advisable to transform Eq. (10) for the damage integral into inequality as

$$\Omega(\mathbf{r}, \tau) = A \int_0^\tau \exp\left[-\frac{E_a}{\Re T(\mathbf{r}, t)}\right] dt \geq 1. \qquad (11)$$

Knowing the temperature distribution in the vicinity of the nanoparticle that is irradiated by a laser light, one can determine on the basis of Eq. (11) the exposure time τ, required to damage locally cell membrane or tissue. As the temperature decreases monotonically with distance from the heated nanoparticle, the execution of the inequality described by Eq. (11) at a distance Δr from the particle will mean automatically that within the layer of thickness $\Delta r = r - R$ of the biological medium around the nanoparticle, the damage condition is obviously achieved. Targeted delivery of nanoparticles to the cell within a tissue allows for selective nanoparticle heating and corresponding thermal impact on the cell in accordance with Arrhenius damage function. The precision of the light/temperature exposure
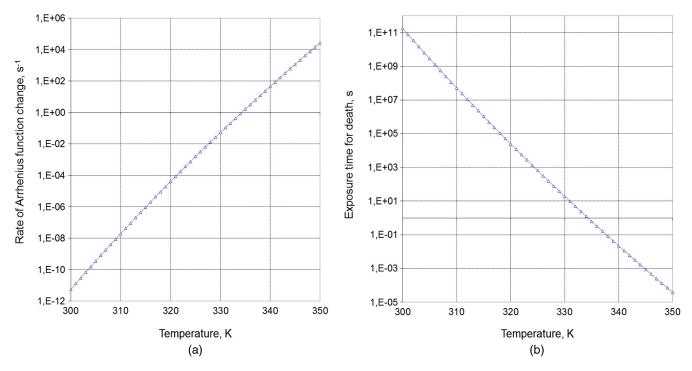
Fig. 6 Dependence of the rate of Arrhenius function change $d\Omega/d\tau$ (a) and exposure time needed for 100%-damage of pig skin versus stationary temperature exposure (b).

needed to induce a particular action is determined by the ability to create the conditions, when smoothly controlled interaction of laser radiation with tissues doped by nanoparticles is provided.

The exposure time τ is the most widespread and robust controlling parameter used for implementation of laser hyperthermia techniques. The calculated topograms of the isoline distribution for τ in the range of 60 to 600 s for different distances Δr apart from the nanoparticle are shown in Fig. 7.

Obtained results show with evidence that in practice, the ensuring compliance of the specific requirements to exposure time is a nontrivial task. The range of admissible values of parameters λ and R occupies only a small area in the coordinate space $(\lambda \times R)$. Often it is similar to a line of small thickness, which indicates a high criticality of providing of laser hyperthermia. Small changes in any of the parameters λ or R will lead to considerable changes in exposure time τ.

Thus, the results shown in Fig. 7(a) (on the surface of the nanoparticle) demonstrate that the admissible variability of nanoparticle size is only in the limits of 2 to 4 nm for the wide range of laser wavelengths from 320 to 600 nm. If size of the nanoparticle is outside these limits, the local damage in a cell or tissue contacting with the nanoparticle comes very quickly at decreasing of nanoparticle radius (subsecond range instead of predetermined minute range), or very slowly within hours of exposure at radius increase. Transition from overheating to underheating becomes practically not controllable. Thus, noncriticality in relation to the wavelength is accompanied by criticality with respect to the radius of the GNP. This is characteristic for curve fragments with small inclination to the horizontal axis.

However, as can be seen in Fig. 7(a), there is a region of parameters: $80 < R < 100$ nm and $615 < \lambda < 660$ nm, where τ isolines rarefied and distributed relatively uniformly over the area of interest. This indicates a lack of criticality with respect to the radius of nanoparticle as well as the laser wavelength.

There is also a second area of noncriticality that corresponds to the wavelength close to 670 nm. The change of nanoparticle radius R from 60 to 75 nm does not result in catastrophic change of exposure τ, while remaining within the prescribed limits. This vertical fragment of curve corresponds to the zone of noncriticality in relation to R and simultaneously to the zone of criticality with respect to λ.

These statements are also important for the problem of polydispersity of used nanoparticles. For better control of photothermal action mediated by plasmonic nanoparticles, monodisperse nanoparticle solutions are preferable. However, polydisperse systems allow one to activate differently sized nanoparticles by the wavelength tuning.

If we set thickness of a layer in surrounding medium with hyperthermia as $\Delta r = 30$ nm (thrice larger than the thickness of cell membrane that complies requirements of cell optoporation),[11–13] the two zones of noncriticality (optimal exposure parameters) are converted to the form shown in Fig. 7(b). The size of the zone corresponding to the 60 to 600 s exposure time is reduced by coordinate R on 12 to 15 nm and decreased in the wavelength range on 20 to 40 nm. At the same time, there is a tendency for optimal R and λ to be decreased.

The further increase of Δr to 120 nm leads to the appearance of the new zone of noncriticality (optimality) in Fig. 7(c), the center of which corresponds to coordinates of SPR. Its special feature is the ability to support exposure time τ in a very narrow range of 300 to 360 s with using nanoparticles of radius 45 ± 5 nm and the laser wavelength of 525 ± 6 nm. The fulfillment of damage conditions in the space around the nanoparticle within 300 nm from its surface may be achievable only for large nanoparticles with a radius of no less than 95 nm and the irradiating wavelength of 520 nm [see Fig. 7(d)]. The general trend of parameter transformation to provide the desired exposure time is as follows: with increasing distance from the
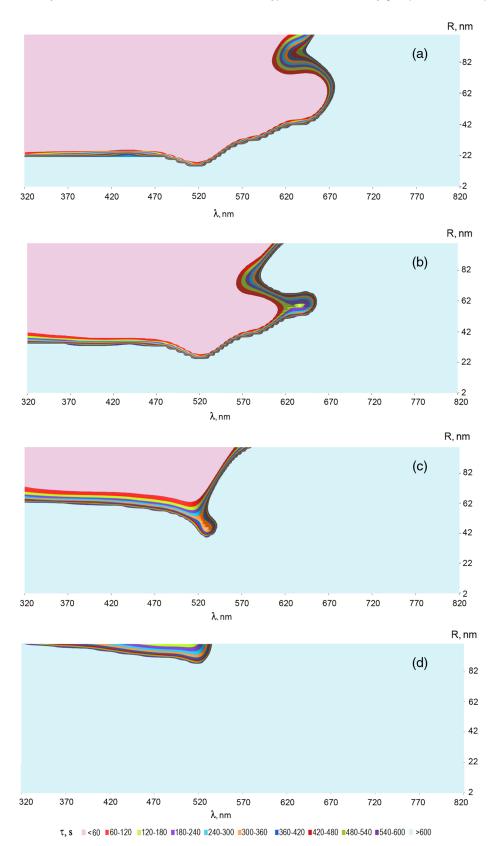
Fig. 7 $(\lambda \times R)$-Topograms for the exposure time τ that provides a local damage in a tissue (pig skin): on the surface of the nanoparticle (a), at a distance of 30 nm apart nanoparticle (b), 120 nm (c), and 300 nm (d).

nanoparticle, the necessary heating/impact conditions are provided only with nanoparticle radius increase and use of a shorter wavelength.

The described technique can be also applicable to study local laser hyperthermia at short pulse irradiation where integration of Eq. (10) should be done for nonstationary temperature fields.[45] To account for more complex nanoparticle shape, such as composite nanoshells, nanorods, nanocages, and nanostars, the adaptive numerical models for calculating temperature fields should be used while the other main stages of the simulation will be retained.

4 Conclusions

These results allow one to have a more general judgment about the significance of the size and acceptable size distribution of GNPs (nanospheres) used for doping of cells and tissues to provide optimal local laser hyperthermia. It was shown that the accuracy of hyperthermia control essentially depends on dimensional factors related to nanoparticle arrangement and size. Adopted conventional criterion for the efficiency of the nanoparticle heating in terms of the nanoparticle absorption ability is not fully determinative. SPR has a significant role only in the certain particular cases. In the coordinate space of the parameters $\lambda \times R$, there are areas of noncriticality, where precise exposure control can be achieved while the requirements for nanoparticle monodispersity are not so strict, the width of size distribution could be up to 15 to 20 nm. Usually, these areas of noncriticality correspond to the nanoparticle size exceeding the size characteristic for efficient SPR.

The proposed methodology based on the developed model for calculation of temperature fields that can be applicable for analysis of local hyperthermia provided by nanoparticles of different shape, including nanoshells,[30–32] nanorods,[6,7,13,33] nanocages,[47] nanostars,[17,18,48] and nanodiscs[49] at CW and pulsed modes of laser irradiation.

References

1. V. V. Tuchin et al., "Protection and treatment of cancer and inflammatory diseases," *J. Biomed. Opt.* **14**(2), 021001 (2009).
2. L. A. Dykman and N. G. Khlebtsov, "Gold nanoparticles in biomedical applications: recent advances and perspectives," *Chem. Soc. Rev.* **41**(6), 2256–2282 (2012).
3. D. G. Cahill et al., "Nanoscale thermal transport. II. 2003–2012," *Appl. Phys. Rev.* **1**, 011305 (2014).
4. V. K. Pustovalov, "Modeling of the processes of laser-nanoparticle interaction taking into account temperature dependences of parameters," *Laser Phys.* **21**, 906 (2011).
5. G. S. Terentyuk et al., "Laser-induced tissue hyperthermia mediated by gold nanoparticles: toward cancer phototherapy," *J. Biomed. Opt.* **14**, 021016 (2009).
6. G. Terentyuk et al., "Gold nanorods with hematoporphyrin-loaded silica shell for dual-modality photodynamic and photothermal treatment of tumors in vivo," *Nano Res.* **7**(3), 325–337 (2014).
7. V. P. Pattani and J. W. Tunnell, "Nanoparticle-mediated photothermal therapy: a comparative study of heating for different particle types," *Laser Surg. Med.* **44**, 675 (2012).
8. J. H. Randrianalisoa et al., "Effects of short-pulsed laser radiation on transient heating of superficial human tissues," *Int. J. Heat Mass Transfer* **78**, 488–497 (2014).
9. M. Waleed et al., "Single-cell optoporation and transfection using femtosecond laser and optical tweezers," *Biomed. Opt. Express* **4**(9), 1533 (2013).
10. B. St-L. Lalonde et al., "Visible and near infrared resonance plasmonic enhanced nanosecond laser optoporation of cancer cells," *Biomed. Opt. Express* **4**(4), 490 (2013).
11. K. Bhattacharyya, S. Mehta, and J. Viator, "Optically absorbing nanoparticle mediated cell membrane permeabilization," *Opt. Lett.* **37**(21), 4474 (2012).
12. Y. Arita et al., "Laser-induced breakdown of an optically trapped gold nanoparticle for single cell transfection," *Opt. Lett.* **38**(17), 3402 (2013).
13. R. Palankar et al., "Nanoplasmonically-induced defects in lipid membrane monitored by ion current: transient nanopores versus membrane rupture," *Nano Lett.* **14**(8), 4273–4279 (2014).
14. V. V. Tuchin, A. Tárnok, and V. P. Zharov, "In vivo flow cytometry: a horizon of opportunities," *Cytometry A* **79A**(10), 737–745 (2011).
15. S. Nangia and R. Sureshkumar, "Effects of nanoparticle charge and shape anisotropy on translocation through cell membranes," *Langmuir* **28**, 17666 (2012).
16. L. A. Dykman and N. G. Khlebtsov, "Uptake of engineered gold nanoparticles into mammalian cells," *Chem. Rev.* **114**(2), 1258–1288 (2014).
17. L. Shao et al., "Plasmonic properties of single multispiked gold nanostars: correlating modelling with experiments," *Langmuir* **28**, 8979 (2012).
18. R. Rodriguez-Oliveros and J. A. Sanchez-Gil, "Gold nanostars as thermoplasmonic nanoparticles for optical heating," *Opt. Express* **20**(1), 621 (2012).
19. V. V. Tuchin, *Tissue Optics: Light Scattering Methods and Instruments for Medical Diagnosis*, 3rd ed., PM 254, SPIE Press, Bellingham, WA (2015).
20. G. F. Baronzio and E. D. Hager, *Hyperthermia in Cancer Treatment: A Primer*, Springer Science+Business Media, New York (2006).
21. K. Li and M. Schneider, "Quantitative evaluation and visualization of size effect on cellular uptake of gold nanoparticles by multiphoton imaging-UV/Vis spectroscopic analysis," *J. Biomed. Opt.* **19**(10), 101505 (2014).
22. E. I. Galanzha et al., "Photoacoustic and photothermal cytometry using photoswitchable proteins and nanoparticles with ultrasharp resonances," *J. Biophotonics* **8**(1–2), 81–93, (2015).
23. D. A. Nedosekin et al., "Super-resolution nonlinear photothermal microscopy," *Small* **10**(1),135–142 (2014).
24. J. Shao et al., "Photothermal nanodrugs: potential of TNF-gold nanospheres for cancer theranostics," *Sci. Rep.* **3**, 1293 (2013).
25. A. Oraevsky and D. Lapotko, "Laser activated nanothermolysis of cells," U.S. Patent 2012/0046593 (2012).
26. J. Elbaz et al., "Powering the programmed nanostructure and function of gold nanoparticles with catenated DNA machines," *Nat. Commun.* **4**, 2000 (2013).
27. V. K. Pustovalov, L. G. Astafyeva, and W. Fritzsche, "Selection of thermo-optical parameter of nanoparticles for achievement of their maximal thermal energy under optical irradiation," *Nano Energy* **2**, 1137–1141 (2013).
28. V. K. Pustovalov, L. G. Astafyeva, and W. Fritzsche, "Plasmonic and thermooptical properties of spherical metallic nanoparticles for their thermoplasmonic and photonic applications," *J. Nanopart.* **2014**, 893459 (2014).
29. V. K. Pustovalov and V. A. Babenko, "Optical properties of gold nanoparticles at laser radiation wavelengths for laser applications in nanotechnology and medicine," *Laser Phys. Lett.* **1**, 516 (2004).
30. Yu. A. Avetisyan, A. N. Yakunin, and V. V. Tuchin, "On the problem of local tissue hyperthermia control: multiscale modelling of pulsed laser radiation action on a medium with embedded nanoparticles," *Quant. Electron.* **40**, 1081 (2011).
31. Y. A. Avetisyan, A. N. Yakunin, and V. V. Tuchin, "Novel thermal effect at nanoshell heating by pulsed laser irradiation: hoop-shaped hot zone," *J. Biophotonics* **5**(10), 734–744 (2012).
32. Y. A. Avetisyan, A. N. Yakunin, and V. V. Tuchin, "Thermal energy transfer by plasmon-resonant composite nanoparticles at pulse laser irradiation," *Appl. Opt.* **51**(10), C88–C94 (2012).
33. F. Ratto et al., "CW laser-induced photothermal conversion and shape transformation of gold nanodogbones in hydrated chitosan films," *J. Nanopart. Res.* **13**(9), 4337–4348 (2011).

34. P. B. Johnson and R. W. Christy, "Optical constants of the noble metals," *Phys. Rev. B.* **6**, 4370 (1972).
35. G. M. Hale and M. R. Querry, "Optical constants of water in the 200-nm to 200-μm wavelength region," *Appl. Opt.* **12**(3), 555–563 (1973).
36. E. A. Coronado and G. C. Schatz, "Surface plasmon broadening for arbitrary shape nanoparticles: a geometrical probability approach," *J. Chem. Phys.* **119**, 3926–3934 (2003).
37. A. Moroz, "Electron mean-free path in a spherical shell geometry," *J. Phys. Chem. C.* **112**(29), 10641–10652 (2008).
38. C. F. Bohren and D. R. Huffman, *Absorption and Scattering of Light by Small Particles*, Wiley, New York (1983).
39. M. H. Niemz, *Laser-Tissue Interactions: Fundamentals and Applications*, 3rd ed., Springer, Berlin, Heidelberg, New York (2007).
40. A. J. Welch and M. J. C. van Gemert, Eds., *Optical-Thermal Response of Laser-Irradiated Tissue*, 2nd ed., Springer Science+Business Media, Berlin, Heidelberg, New York (2011).
41. M. A. Garcia, "Surface plasmons in metallic nanoparticles: fundamentals and applications," *J. Phys. D: Appl. Phys.* **44**, 283001 (2011).
42. X. Huang et al., "Plasmonic photothermal therapy (PPTT) using gold nanoparticles," *Laser Med. Sci.* **23**(3), 217–228 (2008).
43. M. Everts et al., "Covalently linked Au nanoparticles to a viral vector: potential for combined photothermal and gene cancer therapy," *Nano Lett.* **6**(4), 587–591 (2006).
44. G.S. Terentyuk et al., "Cancer laser therapy using gold nanoparticles," in *Lasers for Medical Applications: Diagnostics, Therapy and Surgery*, pp. 659–703, H. Jelinkova, Ed., Electronic and Optical Materials Series No. 37, Woodhead Publishing, Ltd., London (2013).
45. A. N. Yakunin, Y. A. Avetisyan, and V. V. Tuchin, "Scaling of photothermal effects accounting for localization of CW and pulse laser radiation within plasmonic nanoparticles," *Proc. SPIE* **8580**, 85801I (2013).
46. S. L. Jacques, "Ratio of entropy to enthalpy in thermal transitions in biological tissues," *J. Biomed. Opt.* **11**(4), 041108 (2006).
47. B. N. Khlebtsov et al., "Enhanced photoinactivation of Staphylococcus aureus with nanocomposites containing plasmonic particles and hematoporphyrin," *J. Biophotonics* **6**(4), 338–351 (2013).
48. H. Yuan et al., "Plasmonics-enhanced and optically modulated delivery of gold nanostars into brain tumor," *Nanoscale* **6**(8), 4078–4082 (2014).
49. G. M. Santos et al., "Characterization of nanoporous gold disks for photothermal light harvesting and light-gated molecular release," *Nanoscale* **6**, 5718–5724 (2014).

Alexander N. Yakunin is a head of sector for modeling of physical processes in nanoscale structures, the Institute of Precise Mechanics and Control RAS, professor of Saratov State Technical University. His research interests are in the development and application of numerical methods for solving problems of thermal physics, structural mechanics, electrophysics, and analysis of nanostructures. He has authored more than 150 scientific papers, 4 monographs, and 15 patents.

Yuri A. Avetisyan graduated from Saratov State University. Since 1989, he works as senior scientific fellow of laboratory on laser diagnostics of technical and living systems, Inst. of Precise Mechanics and Control, RAS. He has authored more than 70 scientific papers. His research interests focus on the theory of diffraction, theoretical analysis of optical, and temperature fields in nanoplasmonics and nonlinear optics.

Valery V. Tuchin holds the optics and biophotonics chair and is a director of the Research-Educational Institute of Optics and Biophotonics at Saratov State University, head of laboratory on laser diagnostics of technical and living systems, Inst. of Precise Mechanics and Control, RAS. He has authored more than 350 peer-reviewed papers and books. He has been awarded Honored Science Worker of the Russian Federation, SPIE Fellow, the SPIE Educator Award, and Chime Bell Prize of Hubei Province, China. He is a FiDiPro professor of the University of Oulu (Finland), guest professor of HUST (Wuhan) and Tianjin Universities of China, and adjunct professor of the University of Limerick (Ireland) and National University of Ireland (Galway).